PNAS
www.pnas.org

Supplementary Information for

Influence of nuclear quantum effects on the electronic properties of amorphous carbon

Arpan Kundu, Yunxiang Song and Giulia Galli

Corresponding Authors:
Arpan Kundu .
E-mail: arpank@uchicago.edu, arpan.kundu@gmail.com
Giulia Galli.
Email: gagalli@uchicago.edu

This PDF file includes:

Supporting Information Text

Additional Discussions

Atomic coordination. Risplendi *et al* (1) reported that the a-C samples of density 3.25 g cm^{-3} examined in their study contain $\sim 25\%$ 3-fold coordinated C atoms. To determine the coordination number of a C atom they chose a C—C cutoff distance which is slightly larger than the first maximum of the C—C radial distribution function obtained with classical FPMD simulations. Using a cut-off of 1.7 Å, we obtained similar values. This analysis, however, lacks any input from electronic structure calculations as well as the effect of quantum nuclear motion.

We computed the pair correlation function (PCF) between C atoms and maximally localized Wannier function centers (2) (denoted by X) for crystalline diamond as well as amorphous C samples obtained from classical and quantum FPMD simulations at 100 K and 500 K. The results are reported in panels (a) and (b) of Fig. 1 in the main text. Irrespective of whether nuclear quantum effects are included or not, we find that a-C samples have a much broader PCF than that of crystalline diamond due to the presence of elongated and dangling bonds; as expected we also find that the presence of NQEs broadens the distribution of bonds for both crystalline and amorphous C. Following previous studies (3, 4), we define two C sites as bonded if they share a Wannier function center (X) within a given cut-off distance, chosen to correspond to the first minimum of the C—X pair correlation function of diamond. Using this definition of C—C bonds, we obtain a smaller fractions of 3-fold coordinated C atoms in our simulations compared to that reported in Ref. (1); see panels c-d of Fig. 1 in the main text.

For each 3-fold coordinated C atom, we checked whether the C atom is in the same plane defined by its three neighbors. If this condition is satisfied, we identify that C atom as an sp^2 site. For the static structure, i.e., when the atoms are not vibrating, we found that only for the sample with the lowest HOMO-LUMO gap, there are sp^2 sites, and these are in low concentration ($\simeq 2\%$).

Electron-phonon renormalization of mobility gaps. We note that we identified four samples for which by linearly extrapolating the values of the renormalized mobility gaps obtained with classical FPMD simulations to T = 0 K, we recovered the computed, static mobility gap within 40 meV. This indicates that for these samples the classical ZPRs are almost zero, as expected. In contrast, we identified three samples with static mobility gaps of 4.27 eV, 4.41 eV and 4.92 eV, for which larger differences of 136 meV (Fig. 5b in main text), 125 meV (Fig S5, panel b) and -388 meV (Fig. 5d in main text), respectively, were observed. For these samples, a much larger broadening of the electronic density of states below the chosen IPR threshold value is observed even at 100K. This broadening originates from the presence of localized single particle states with high IPR values, that lie within the delocalized bulk states. For example, in Fig. 4 of the main text, for the static a-C structure (black stars), we see two nearby conduction band states ($E - E_{\mathrm{Fermi}} \sim 2$eV) with IPR values 0.007 and 0.001. The former is a trapped state whose localization varies as a function of nuclear motion, and which partially contributes to the ensemble average of the mobility gap. This effect, which is absent when the nuclei are frozen, is included in the linear extrapolation procedure, leading to a non-zero value of the extrapolated classical ZPR. We also note that, when NQEs are included, the Viña extrapolation also includes such effects, and consequently, for the sample with the largest gap (Fig. 5d in main text), we observe a rather large ZPR of -800 meV, though the difference between quantum and classical results extrapolated to T = 0 K is only -400 meV.

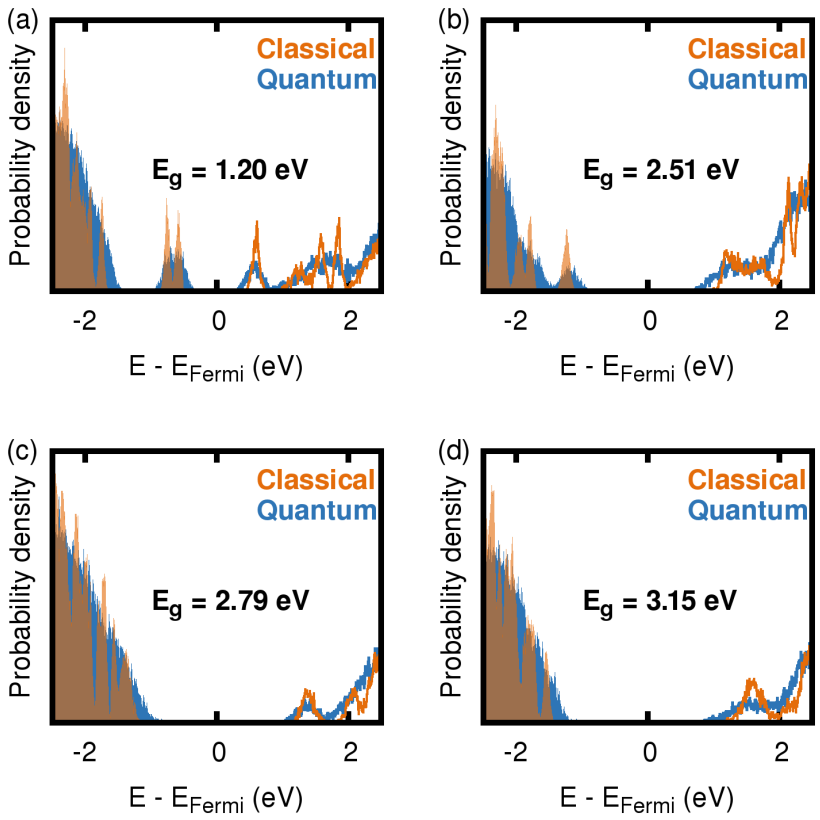

Fig. S1. Electronic density of states (EDOS) at 100 K computed with classical FPMD ("Classical") and quantum FPMD ("Quantum") simulations for four representative samples with static HOMO-LUMO gap of (a) 1.20 eV, (b) 2.51 eV (c) 2.79 eV, and (d) 3.15 eV. Shaded region represents the valance band and unshaded region represents the conduction bands.

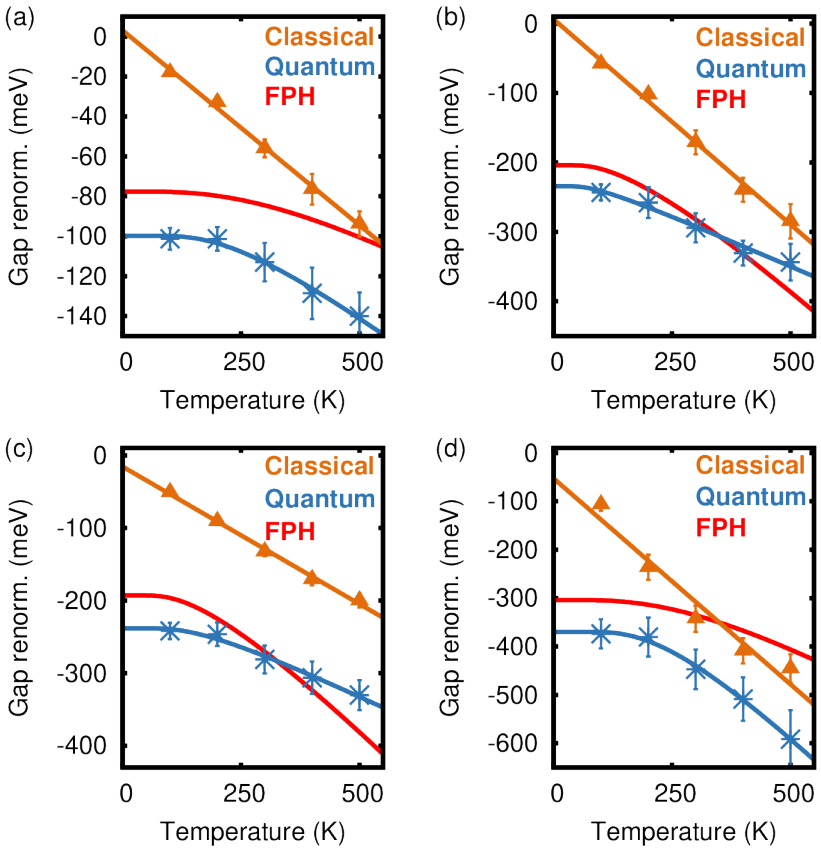

Fig. S2. HOMO-LUMO gap renormalization due to electron-phonon interaction as a function of temperature for four different a-C samples of density 3.25 g/cm^3. The static HOMO-LUMO gaps for these samples are: (a) 1.203 eV, (b) 2.511 eV, (c) 2.786 eV and (d) 3.149 eV, respectively; see also Table 1 in main text. The orange and blue symbols are the results of FPMD simulations performed with a (i) classical and (ii) quantum thermostat, respectively.The blue (orange) lines are the Viña (linear) model fit (5) of the quantum (classical) results, while the red lines are the results obtained with frozen phonon harmonic (FPH) calculations.

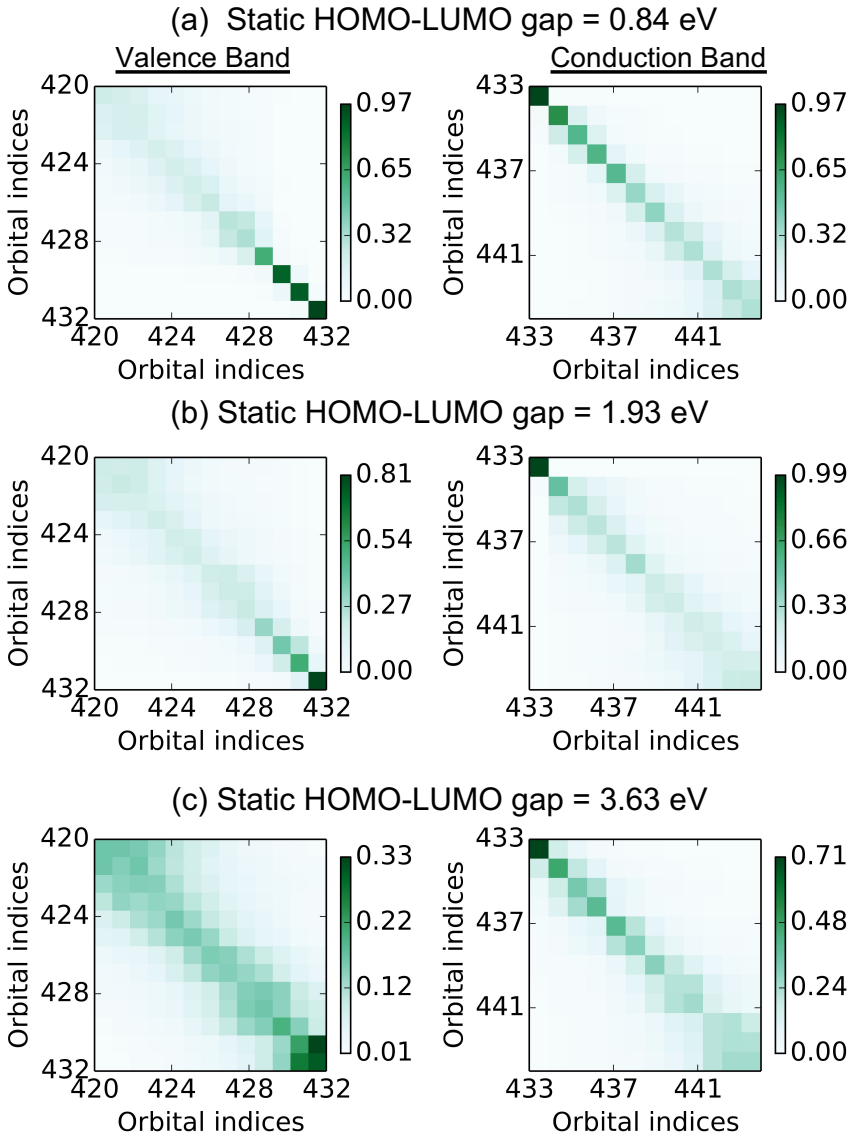

Fig. S3. Ensemble averaged overlap matrix elements for 13 occupied orbitals (orbital indices 420-432, shown in left panel) and 12 unoccupied orbitals (orbital indices 433-444, shown in right panel) close to the Fermi level. The overlap matrix elements are computed between the orbitals of a MD snapshot and those of its closest local minimum and then averaged over 700 snapshots collected every 50 steps (25 fs) of quantum FPMD simulations at 100 K. Top to bottom (a-c) panels show the results for the same samples showns in Fig. 3, panels a-c of the main text.

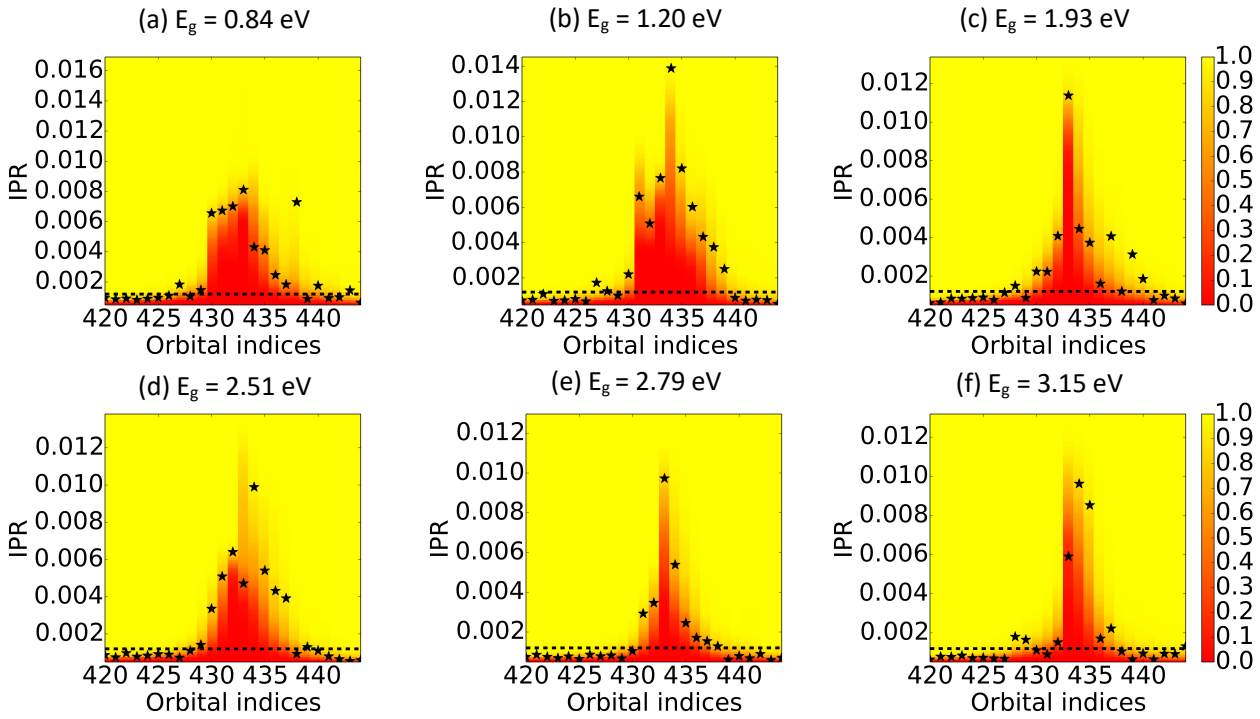

Fig. S4. Cumulative probability distribution (less than type) of the inverse participation ratios (IPR) as a function of single particle orbital indices for six representative amorphous carbon samples with increasing static HOMO-LUMO gaps (E_g). The distribution is computed based on 500 snapshots obtained from quantum FPMD simulations performed at 500 K. Orbitals with indices 432 and 433 represent the valence band maximum (VBM or HOMO) and conduction band minimum (CBM or LUMO), respectively. The Colormap represents the cumulative probability (less than type), i.e., the probability of obtaining the IPR below the value shown on the Y-axis. Black stars represent the IPR and orbital indices when atoms are at rest. The black dotted line shows the chosen IPR cutoff for the calculation of mobility gaps.

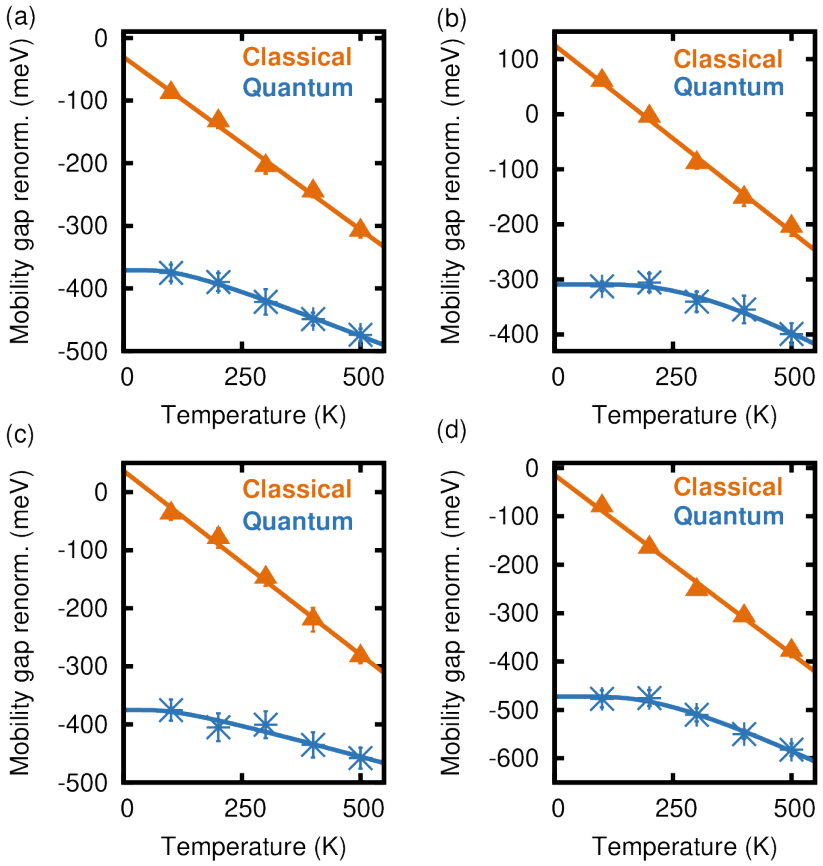

Fig. S5. Temperature dependence of electron phonon renormalization of mobility gaps obtained from classical and quantum FPMD simulations for four different amorphous C samples with density 3.25 g. cm.$^{-3}$. The static HOMO-LUMO and mobility gaps (in parentheses) for these samples are: (a) 2.786 eV (4.789 eV), (b) 1.930 eV (4.411 eV), (c) 3.149 eV (4.488 eV), and (d) 1.203 eV (4.746 eV), respectively; see also Table 1 in the main text. The symbols represent the simulation results whereas the solid lines represent the simulated results fitted with the linear (classical) and Viña (quantum) (5) models.

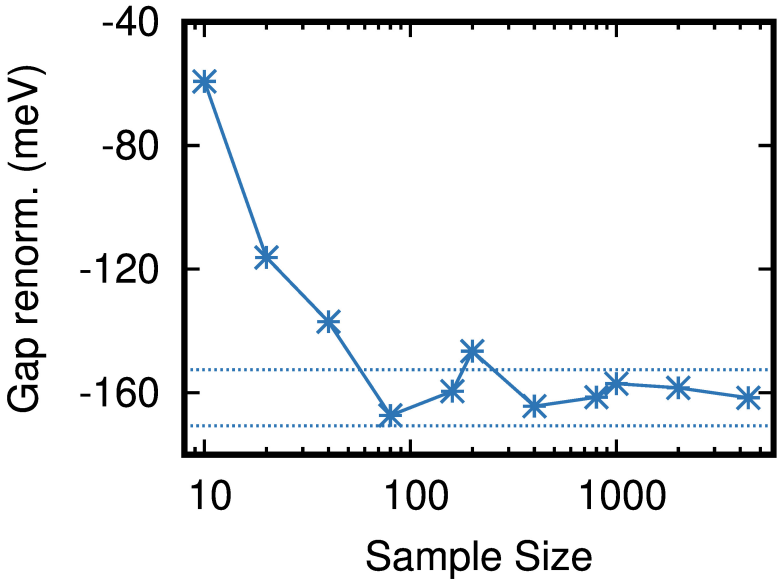

Fig. S6. Convergence of HOMO-LUMO gap renormalization with respect to the chosen sample size from a 17.5 ps long quantum FPMD trajectory (production run) at 100 K. The static HOMO-LUMO gap for that sample is 1.930 eV. Sample sets are chosen such that for a particular set, the time interval between two successive samples are same. The dashed line is the estimated statistical uncertainties for the sample set with 4375 samples. We note that more than 100 samples are at least required to converge the gap renormalization.

References

1. F Risplendi, M Bernardi, G Cicero, JC Grossman, Structure-property relations in amorphous carbon for photovoltaics. *Appl. Phys. Lett* **105**, 043903 (2014).
2. N Marzari, AA Mostofi, JR Yates, I Souza, D Vanderbilt, Maximally localized wannier functions: Theory and applications. *Rev. Mod. Phys.* **84**, 1419–1475 (2012).
3. D McCulloch, et al., Wannier function analysis of tetrahedral amorphous networks. *Diam. Relat. Mater.* **12**, 2026–2031 (2003) Proceedings of the 8th International Conference on New Diamond Science and Technology (ICNDST-8).
4. P Fitzhenry, MMM Bilek, NA Marks, NC Cooper, DR McKenzie, Wannier function analysis of silicon carbon alloys. *J. Phys.: Condens. Matter* **15**, 165–173 (2002).
5. L Viña, S Logothetidis, M Cardona, Temperature dependence of the dielectric function of germanium. *Phys. Rev. B* **30**, 1979–1991 (1984).